LA-UR-96-3015
CONF-9608133--3

TITLE: ELECTRON BEAMLINE DESIGN FOR THE LOS ALAMOS NATIONAL LABORATORY 1 KW FEL

AUTHOR(S): Richard Lee Sheffield AOT-4

SUBMITTED TO: FEL 96 Conference
Rome, Italy
August 26-31, 1996

Los Alamos
NATIONAL LABORATORY

Form No. 836 R5
ST 2629 10/91

DISCLAIMER

Electron beamline design for the Los Alamos National Laboratory 1 KW FEL*

R. L. Sheffield
Los Alamos National Laboratory, Los Alamos, NM (USA)

Abstract

This paper describes the electron beam simulations for a 1 kW average power FEL. The experiment utilizes the existing AFEL accelerator. An expected 6% total efficiency of electron beam power to optical power gives 17 kW of electron beam power for 1 kW of optical power. A constraint on the beamline design is that the FEL electron beamline and optical components must fit on the existing AFEL 6 ft. high by 10 ft. long optical table. The components include electron beam diagnostics, a 2 meter long wiggler, bending magnets, and optical feedback components.

The electron beam design point is 300 A peak current, 17 MeV energy, 7.5 π mm-mrad effective normalized rms emittance and 6 nC micropulse charge. The electron beamline will have greater than 99% transmission. The wiggler will have weak (natural) two plane focusing to maintain the electron beam size in the long wiggler. The beamline after the wiggler has to transport a beam with a 14 to 18 MeV energy spread and an average energy of 16 MeV.

* This work was conducted under the auspices of the U. S. Department of Energy, supported (in part) by funds provided by the University of California for the conduct of discretionary research by Los Alamos National Laboratory.

1. Introduction

The performance parameters required for the 1 kW experiment [1] are 300 A peak current, 17 MeV energy, 7.5 π mm-mrad emittance and 6 nC micropulse charge. The experiment utilizes the existing AFEL accelerator [2]. The electron and optical beamline must fit on the vertical 6 ft high by 10 ft long optical table and have room for a 2 meter wiggler and feedback optics. A schematic of the layout is shown in reference 1.

The following design meets the above mentioned performance requirements. The design encompasses two operation modes. The first mode is operation without a wiggler for accelerator characterization. The second mode is operation with a wiggler. The two matching modes require different solenoid and quadrupole settings.

The wiggler will have weak (natural) two-plane focusing to maintain the electron beam size in the long wiggler. The beam is focused into the wiggler with two quad doublets. A limiting aperture of 2.0 mm radius is positioned 10 cm before the wiggler entrance (this represents the hole in the mirror). With the present design, less than 1% of the particles hit the aperture. The wiggler has 50 2-cm uniform periods and 50 2-cm tapered periods. The magnetic field is 7000 gauss with a 0.59 cm gap in the uniform section going to a 0.95 cm gap at the end of the tapered section. After the wiggler, a quad doublet focuses the electrons into a 120° bend. At FEL saturation simulations give an electron beam that has a 14 to 18 MeV energy spread with an average energy of 16 MeV.

To maximize the peak current, a large area photocathode is required. The present AFEL cathode plug has a 8 mm radius, thus limiting the maximum cathode radius to 7 mm. The extra 1 mm keeps photocathode material away from the plug edges.

2. Accelerator Simulation

For the simulations, the accelerator is run at a 20° (from the zero crossing) electron bunch injection phase and 6 nC pulse charge. Experimentally, the accelerator phase will be set for minimum energy spread (measured to be within 5° of simulation phase). The main solenoid current setting depends on if the wiggler is installed. Without the wiggler, the solenoid is set to 262 A. With the wiggler, the solenoid is set to 292 A. For matching the beam to the wiggler, the solenoid field will significantly affect the quadrupole matching conditions. With no wiggler, a larger beam (smaller solenoid setting) is required since the beam is large in the drift where the wiggler would have been.

Since a perfect temporally square electron pulse is not possible, the performance of the accelerator for three different laser temporal profiles was investigated. The three temporal profiles are shown in Figure 1.

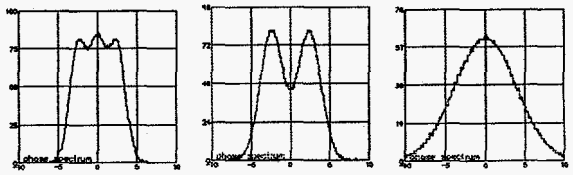

Figure 1. Drive laser pulse temporal formats. The FWHM and total charge for the three pulses are the same. The horizontal scale is 5 degrees of 1.3 GHz per division.

The emittance 25 cm downstream of the accelerator depends on how much of the longitudinal distribution is used (Figure 2). For 80% of the charge (10% of the beam is chopped from both ends), the rms emittance is less than 7 π mm-mrad. The middle 10% of the pulse has an rms emittance less than 4 π mm-mrad. The cathode thermal

emittance will contribute as square root of sum of squares and is not taken is not account.

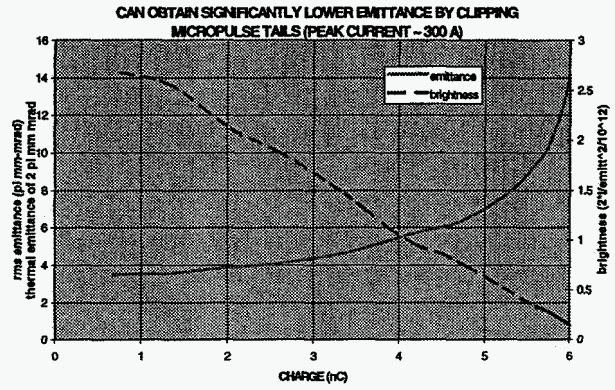

Figure 2. Clipping longitudinal distribution simultaneously from both ends of micropulse for the triple-gaussian input laser pulse.

2.1 Simulations with Triple Gaussian Input Laser Pulse.

This simulation uses three longitudinally displaced gaussians as the input pulse (Figure 3). Each gaussian has a temporal width of 3.1 ps, and each gaussian is separated by 5.2 ps.

The emittance and brightness for this input were shown in Figure 2. The peak current from the gun is 320 A.

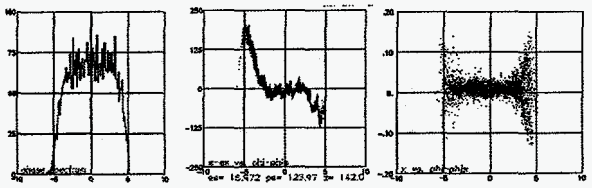

Figure 3. Beam characteristics downstream of the linac for a triple gaussian input pulse. The left is the temporal profile of the pulse, the middle is the energy versus phase, and the right is electron radius versus phase at the wiggler entrance. The horizontal scale is 5 degrees of 1.3 GHz per division. The vertical scales are particle number per bin, 100 KeV, and 0.10 cm for the left, center, and right figure, respectively

The front and back of the electron pulse do not contribute substantially to the FEL interaction. To properly match the electron beam to the wiggler requires ignoring the particles at the front and back of the pulse. Figure 4 shows the matching of the electron beam into the wiggler for all the particles in the pulse and for a pulse with 10% chopped from the front and back of the pulse. Even though the front and back particles have a large oscillation amplitude of nearly 4 mm peak to peak, those particles are still well within the 5.9 mm wiggler gap.

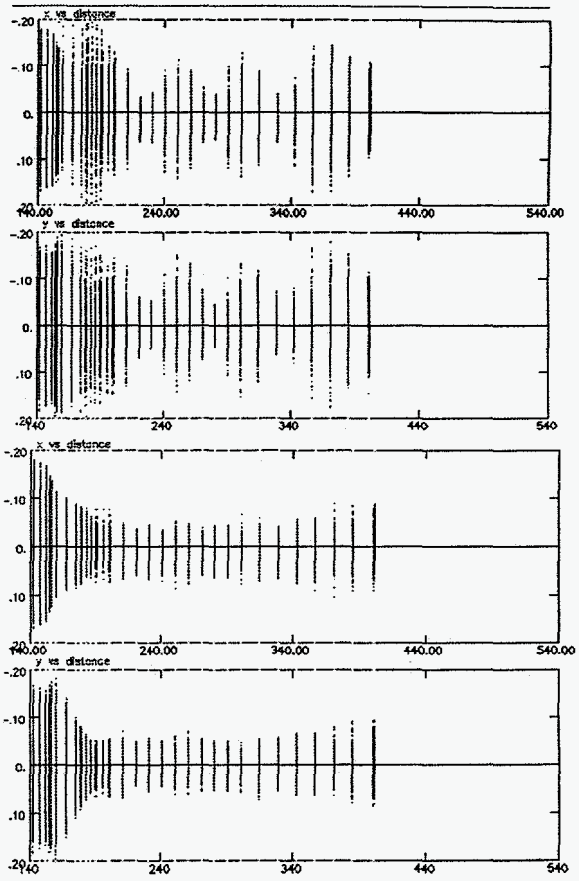

Figure 4. The x and y extent of particles in the wiggler. The upper figure is the x extent without chopping, the second from the top is the y extent without chopping, the second from the bottom is the x extent with chopping 10% from both ends of the longitudinal distribution, and the bottom figure is with chopping. The wiggler is from 200 to 401 cm. The horizontal scale is 140 cm to 540 cm. The vertical scale goes from -0.2 cm to 0.2 cm.

2.2 Simulations with Double Gaussian Input Laser Pulse.

This simulation uses two longitudinally displaced gaussians as the input pulse (Figure 1). The gaussian width and separation are set to give roughly the same output pulse temporal shape from the accelerator (Figure 5) as for the above triple gaussian pulse. All of the quad values for matching into the wiggler are the same as those for the above three-gaussian input pulse case.

A nice feature of the AFEL is that large perturbations in the input amplitude are smoothed out as the pulse is accelerated because of longitudinal space charge forces. However, those longitudinal forces do move particles longitudinally, and so the bunch has a larger energy spread compared to a three gaussian bunch (Figure 3). The effect of this type of energy spread on the FEL performance is not obvious since the energy spread is more accurately an

energy shift with time. For this case, the energy spread is still within acceptable limits (<0.7%). The emittance is also acceptable, with the emittance for the middle 80% less than 7 π mm-mrad and 12 π mm-mrad for the whole pulse. The beam loss for a 4 mm diameter mirror hole is 1.0%.

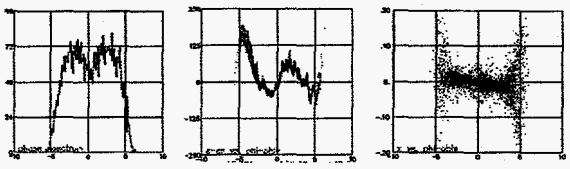

Figure 5. Beam characteristics downstream of the linac for a double gaussian input pulse. The left is the temporal profile of the pulse, the middle is the energy versus phase, and the right is electron radius versus phase at the wiggler entrance. The scales are the same as in Figure 3.

2.3 Simulation with Single Gaussian Input Pulse.

As expected, a gaussian pulse is all wings and so varies considerably in radius and divergence over the duration of the pulse. The average emittance is around 10 π mm-mrad with chopping and 20 π mm-mrad for the whole beam.

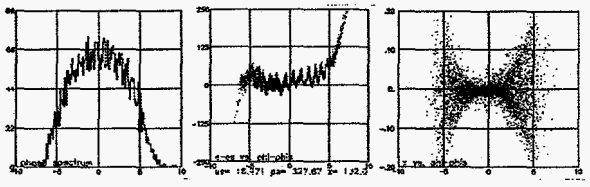

Figure 6. Beam characteristics downstream of the linac for a single gaussian input pulse. The left is the temporal profile of the pulse, the middle is the energy versus phase, and the right is electron radius versus phase at the wiggler entrance. The scales are the same as in Figure 3.

3. Simulation after Accelerator and through Wiggler.

The wiggler is assumed to have equal focusing in x and y. The beam is focused into the wiggler with two quad doublets. A limiting aperture of 2.0 mm radius is positioned 10 cm before the wiggler entrance (this represents the hole in the mirror).

Since most of the highly diverging particles are located in the 10% at the bunch ends (Figure 2), the quadrupole matching condition is determined by transporting the chopped beam to the entrance of the wiggler and using TRACE to initially determine the correct quad values.

The wiggler has 50 2-cm uniform periods and 50 2-cm tapered periods. The magnetic field is 7000 gauss with a 0.59 cm gap in the uniform section going to a 0.95 cm gap at the end of the tapered section. After the wiggler, a quad doublet focuses the electron beam into the 120° bend.

4. Design of Bending Magnet/Spectrometer.

The 120° bend has a 35° entrance and -30° exit edge angle. An energy spectrometer screen is located close to the end plane of the 120° bend. The edge angles have been chosen to simultaneously focus the electron beam at the exit plane of the spectrometer and enable the beam to be transported the beam dump. At the maximum interaction, the FEL will cause the electron energy distribution to range from 14 to 18 MeV. The magnet is schematically shown in Figure 8.

At the maximum interaction, the FEL interaction will cause the electron energy distribution to range from 14 to 18 MeV. An rf cavity after the wiggler is used in the simulation to generate the large energy slew as well as to shift the energy centroid to 16 MeV. The spectrometer magnet is set for 16 MeV. The linear energy spread in Error! Reference source not found. shows the x and y distribution on the screen with a 4 MeV energy spread. This is not the expected energy distribution for the FEL and is used only to demonstrate 100% beam transport to the beam dump.

A spectrometer magnet pole piece that has the correct bend and focusing properties is shown in Figure 7.

A quad triplet focuses the beam into the beam dump. After the quads, a 30° bending magnet will bend the beam into the existing beam dump.

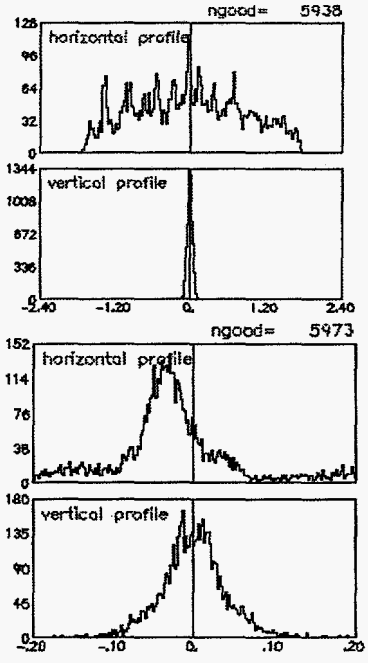

Figure 7. Energy distribution with (upper) and without (lower) an FEL interaction at energy spectrometer screen location. The horizontal scale is -2.4 cm to 2.4 cm on the upper two figures and -0.2 cm to 0.2 cm for lower two figures. The energy distribution in the left horizontal profile figure goes from 14.1 to 18.1 MeV. The expected horizontal resolution is less than 0.3% at 16 MeV.

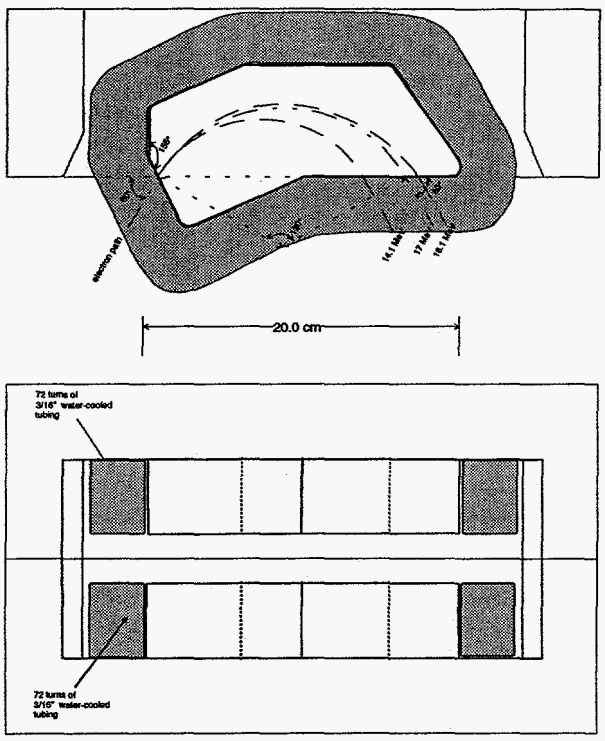

Figure 8. Spectrometer magnet for electron beam. Pole piece of spectrometer magnet with correct edge focusing. For 17 MeV particles and a 9 cm orbit radius, a 6.5 kg field is required.

5. Sensitivity to Operating Parameters

This design is insensitive to variations in the main system parameters. The insensitivity comes about for two main reasons. The first reason is that the beamline design is very simple with few components. This design has no bunch compressor basically eliminating a significant dependency on phase and energy. Similarly, current fluctuations that result in energy variations due to wakefields or beam loading in the accelerator also do not affect performance. The second reason is the ameliorating effect of the photoinjector physics on input fluctuations. Thus fluctuations in the input parameters result in relatively smaller variations in the output beam characteristics.

In the photoinjector the space charge forces act to average local variations inside a micropulse. So, in this design a square pulse is not significantly different from a double gaussian with a 40% amplitude fluctuation in the middle of the pulse. These effects do not apply to a purely gaussian (in time) pulse because there are no balancing effects on the front and back of a micropulse. A single gaussian pulse is basically all wings and gives significantly poorer performance. The sensitivities to operating parameters are summarized in Table 1. Table 1 does not include emittance contribution due to cathode thermal temperature.

Case	Change	Full ε	Chopped ε	I	R
3-gaussian	0	11	4.6	322	0.14-0.19
2-gaussian	0	12	5.3	322	0.14-0.20
1-gaussian	0	20	12		
charge	+5 %	13	5.3	331	0.14-0.20
charge	+10 %	13	5.3	340	0.13-0.22
phase	+2°/1°	13	5.4	326	0.14-0.20
phase	+10°/5°	13	6.5	308	0.11-0.30
linac energy	+2 %	12	5.0	333	0.14-0.19

Table 1. Sensitivity of matching to the wiggler for different operating cases. The emittances "ε"are normalized and the units are π mm-mrad. The chopped emittance is calculated by using a 15 ps wide temporal window in the PARMELA simulation to chop the ends of the micropulse 20 cm after the accelerator. This corresponds to 78% of the particles or 5 nC of charge for most cases. The column "I" is the average current in amps for chopped portion of the pulse. The beam radius "R" column is the range in the rms radius in mm for the uniform section of the wiggler. The FELIX simulation assumes a perfectly matched beam with an 0.19 mm rms radius. The two numbers in the "change" column for phase are injection phase change and resulting phase shift after the accelerator, respectively. The simulations predict that an increase in phase causes a decrease in current (rf bunch compression effect). In practice, the current will increase with increasing phase because a field increase at the cathode leads to an increase in photocathode quantum efficiency.

References

[1] D. C. Nguyen et al., these proceedings.
[2] D. C. Nguyen et al., Nucl. Inst. and Meth. A 358 (1995) 27-30.